Confinement transitions in TJ-II under Li-coated wall conditions

2009 Nucl. Fusion 49 104018

(http://iopscience.iop.org/0029-5515/49/10/104018)

IOP Publishing and International Atomic Energy Agency Nuclear Fusion
Nucl. Fusion **49** (2009) 104018 (10pp) doi:10.1088/0029-5515/49/10/104018

Confinement transitions in TJ-II under Li-coated wall conditions

J. Sánchez, M. Acedo, A. Alonso, J. Alonso, P. Alvarez, E. Ascasíbar, A. Baciero, R. Balbín, L. Barrera, E. Blanco, J. Botija, A. de Bustos, E. de la Cal, I. Calvo, A. Cappa, J.M. Carmona, D. Carralero, R. Carrasco, B.A. Carreras[1], F. Castejón, R. Castro, G. Catalán, A.A. Chmyga[2], M. Chamorro, L. Eliseev[3], L. Esteban, T. Estrada, A. Fernández, R. Fernández-Gavilán, J.A. Ferreira, J.M. Fontdecaba, C. Fuentes, L. García[4], I. García-Cortés, R. García-Gómez, J.M. García-Regaña, J. Guasp, L. Guimarais[5], T. Happel, J. Hernanz, J. Herranz, C. Hidalgo, J.A. Jiménez, A. Jiménez-Denche, R. Jiménez-Gómez, D. Jiménez-Rey, I. Kirpitchev, A.D. Komarov[2], A.S. Kozachok[2], L. Krupnik[2], F. Lapayese, M. Liniers, D. López-Bruna, A. López-Fraguas, J. López-Rázola, A. López-Sánchez, S. Lysenko[3], G. Marcon, F. Martín, V. Maurin[3], K.J. McCarthy, F. Medina, M. Medrano, A.V. Melnikov[3], P. Méndez, B. van Milligen, E. Mirones, I.S. Nedzelskiy[5], M. Ochando, J. Olivares, J.L. de Pablos, L. Pacios, I. Pastor, M.A. Pedrosa, A. de la Peña, A. Pereira, G. Pérez, D. Pérez-Risco, A. Petrov[3], S. Petrov[6], A. Portas, D. Pretty, D. Rapisarda, G. Rattá, J.M. Reynolds[7], E. Rincón, L. Ríos, C. Rodríguez, J.A. Romero, A. Ros, A. Salas, M. Sánchez, E. Sánchez, E. Sánchez-Sarabia, K. Sarksian[8], J.A. Sebastián, C. Silva[5], S. Schchepetov[8], N. Skvortsova[8], E.R. Solano, A. Soleto, F. Tabarés, D. Tafalla, A. Tarancón[7], Yu. Taschev[5], J. Tera, A. Tolkachev, V. Tribaldos, V.I. Vargas, J. Vega, G. Velasco, J.L. Velasco[7], M. Weber, G. Wolfers and B. Zurro

Laboratorio Nacional de Fusión, Asociación EURATOM/CIEMAT, 28040, Madrid, Spain
[1] BACV Solutions Inc., Oak Ridge, TN 37830, USA
[2] Institute of Plasma Physics, NSC KIPT, 310108 Kharkov, Ukraine
[3] Institute of Nuclear Fusion, RNC Kurchatov Institute, Moscow, Russia
[4] Universidad Carlos III, 28911 Leganés, Madrid, Spain
[5] IPFN, As. EURATOM/IST, Lisbon, Portugal
[6] A.F. Ioffe Physical Technical Institute, 26 Polytekhnicheskaya, St Petersburg, Russia
[7] BIFI: Instituto de Biocomputación y Física de Sistemas Complejos, Universidad de Zaragoza, 50009-Zaragoza, Spain
[8] General Physics Institute, Russian Academy of Sciences, Moscow, Russia

E-mail: joaquin.sanchez@ciemat.es

Received 5 December 2008, accepted for publication 10 June 2009
Published 10 September 2009
Online at stacks.iop.org/NF/49/104018

Abstract
This paper presents the latest results on confinement studies in the TJ-II stellarator. The inherently strong plasma–wall interaction of TJ-II has been successfully reduced after lithium coating by vacuum evaporation. Besides H retention and low Z, Li was chosen because there exists a reactor-oriented interest in this element, thus giving special relevance to the investigation of its properties. The Li-coating has led to important changes in plasma performance. Particularly, the effective density limit in NBI plasmas has been extended reaching central values of $8 \times 10^{19}\,\mathrm{m}^{-3}$ and $T_e \approx 250$–$300\,\mathrm{eV}$, with peaked density, rather flat T_e profiles and higher ion temperatures. Due to the achieved

density control, a second type of transition has been added to the low density ones previously observed in ECRH plasmas: higher density transitions characterized by the fall in Hα emission, the onset of steep density gradient and the reduction in the turbulence; which are characteristics of transition to the H mode. Confinement studies in ECH plasmas indicate that lowest order magnetic resonances, even in a low shear environment, locally reduce the effective electron heat diffusivities, while Alfven eigenmodes destabilized in NBI plasmas can influence fast ion confinement.

PACS numbers: 52.25.Fi, 52.40.Hf, 52.55.Hc

(Some figures in this article are in colour only in the electronic version)

1. Introduction

TJ-II is a stellarator of the heliac type, characterized by its high flexibility and its almost flat rotational transform profile [1]. TJ-II is provided with a central conductor composed of two coils: a helical and a circular one. By changing the currents that circulate through these coils, it is possible to modify the plasma shape as well as the rotational transform. This capability has been exploited mainly in ECRH plasmas with a focus on the effect of low order rational values of the rotational transform on plasma profiles. The central conductor is allowed out of the vacuum vessel by means of a helical groove that surrounds its outer surface. It acts as a helical limiter, defining the last closed magnetic flux surface (LCFS). The plasma wall interaction is therefore maximum at the groove inner surface, which can be very close to the magnetic axis (about 12–14 cm, depending on the configuration), thus provoking a strong recycling and possible impurity influx. Several strategies to solve this problem have been attempted, but the last and most successful has been coating the inner walls of TJ-II with Li. Compared with other low Z coating elements such as Be, C and B, Li is a very attractive element due to its very low radiation power, strong H retention as well as strong O getter activity and excellent results have been achieved recently in tokamaks [2], with positive impact on energy confinement [3], as has been predicted [4]. Moreover, research on Li properties has evinced strong interest in the liquid lithium based divertors that are envisaged for future reactors. In this work, the operation of a stellarator, the TJ-II Heliac, with lithium-coated walls is described. The Li-coating implies an important reduction in sputtering and recycling. The most relevant changes in plasma performance and confinement characteristics associated with the new wall scenario are described and analysed in terms of enhanced impurity and particle control. Beyond the specific TJ-II achievements, research on Li-coated wall properties is an outstanding topic in itself, since plasma–wall interaction issues are paramount in achieving fusion plasmas with high purity, controlled density and high confinement. The interaction with the first wall, which is reached by charge exchange (CX) neutrals, photons and some more or less tenuous plasma, is considered to contribute to the plasma impurity content as much as wetted areas do.

Stellarator plasmas show distinct features in their interaction with surrounding materials in comparison with tokamaks. Stellarators do not present disruptions, type I ELMs or MHD-driven density limit [5], which make them more reliable for reactor operation. However, they present a significantly higher aspect ratio thus offering a less favourable area to volume ratio in terms of impurity and particle control. Therefore, several specific divertor concepts have been developed for stellarators with reasonable success [6]. To date the concept of a flux expansion divertor [7] has not been explored experimentally but theoretical studies are underway in TJ-II [8].

Transport is an important concern in fusion plasmas and therefore in TJ-II experiments. This topic has been studied from different perspectives, both in ECH and NBI plasmas although the database of the former is much larger and more systematic. In particular, TJ-II is quite well suited for studying the effect of magnetic resonances in plasma profiles and transport. This is of general importance in the design of reactors based on the stellarator concept. The ability of magnetic islands or stochastic zones to modify transport represents both a threat for good confinement and a potential tool for confinement control. The close interrelation between particle radial fluxes, magnetic topology and transport in stellarators still poses important questions, and their understanding may alleviate some constraints on the design of, especially, low shear devices. Likewise, momentum transport physics and its relation to turbulence is another unresolved ingredient in confinement studies. The transport properties of the plasma edge region, which determine the global quality of plasma confinement, show a systematic link between fluctuations, perpendicular and parallel plasma flows, and transport, particularly near the threshold parameters for confinement transitions. These transitions, which in TJ-II ECRH plasmas can be either spontaneous or biasing driven, display long-range correlations within a magnetic flux surface, in line with the concepts of zonal flow development with Reynolds-stress drive.

In NBI plasmas, destabilized Alfvén eigenmodes (AEs) can influence fast ion confinement and this line of research has been put forward in recent TJ-II experimental campaigns.

Finally, NBI operation with Li-coating has allowed, for the first time in TJ-II, a spontaneous confinement improvement characterized by a reduction in both Hα and broadband fluctuations, as is typical of L- to H-mode transitions. A first estimate of the power threshold scaling agrees with the general trends found in other devices.

This paper presents an overview of experimental results with emphasis on the new TJ-II wall conditions. Remarkably, a new regime for TJ-II operation, with stationary NBI discharges has been achieved by drastically reducing wall recycling via lithium coating. The presentation of Li coating techniques and the properties of the plasma in these new conditions are described in section 2. Section 3 is devoted to the main features

observed in confinement properties: in ECRH plasmas, an important role of the magnetic topology has been uncovered through power balance transport analysis (section 3.1); also, edge studies have shown the formation of $E \times B$ sheared flows and their influence in confinement and turbulence properties (section 3.2); in NBI plasmas, transitions with the typical signatures of the L–H confinement transition have been found (section 3.3) as well as some influence of AEs on fast ion confinement (section 3.4). The summary of the results is given in section 4.

2. Plasma operation with Li-coated walls

The design of the TJ-II vacuum chamber imposes specific plasma–wall interaction issues that have strong influences on confinement: the helical limiter, where most of the recycling and impurity release occurs, is physically close to the plasma centre and therefore the plasma–wall interaction control is a key element in TJ-II operation. The effect of Li-coated walls on plasma performance can be ascribed to the associated changes in recycling, radiated power and impurity penetration, all of these having a direct impact on particle and energy confinement. In previous experimental campaigns, experience with TJ-II plasmas came from ECH (normally with line densities in the range 0.4 to 0.9×10^{19} m^{-3}) and NBI discharges with boronized wall conditions.

In the most recent experimental campaign, the TJ-II stellarator was coated with lithium [9]. The technique used for lithiumization is evaporation using ovens and the Li is homogenized in the vessel walls by the plasma which is seen to distribute the Li. The choice of lithium was motivated mainly by its high efficiency for H retention, its low Z and by the current interest in this element, in particular for liquid divertor concepts. Lithium coating has led to important changes in plasma performance [10]. Particularly conspicuous has been the strong decrease in recycling associated with the new wall conditions, but also in impurity content, with direct impact on radiative losses and total energy confinement, as expected in a first-wall dominated plasma–wall interaction device. The O gettering is still maintained by the boron layer that is deposited under the Li one. The edge radiation is observed to fall, which avoids the power imbalance that produces the low radiation collapse. Changes in the shot by shot fuelling characteristics as well as in the total particle inventory compatible with good density control and plasma reproducibility under ECRH scenarios have been recorded after the Li deposition. Thus, a rise by a factor 2 to 3 in the fuelling rate at constant density compared with the B-coated walls is recorded, and even a higher factor is estimated for the allowed H inventory at the walls. These changes are mirrored in the radiation and edge radial profiles, mostly ascribed to the replacement of the dominant impurity at the edge: the Li-cooling rate properties are much more favourable than the ones of the usual impurities in TJ-II. The new wall conditions lead to the extension of the effective density limit in NBI heating scenarios and to stationary NBI plasmas. First transport estimates on these plasmas indicate much better general confinement properties. Central electron densities up to 8×10^{19} m^{-3} with electron temperatures of 250–300 eV have been recorded, with peaked densities, rather flat T_e profiles and ion temperatures up to 150 eV. Therefore an important sharing of the available plasma energy takes place between the two main species.

Even though total radiation could account for half of the injected power in some instances, the development of a radiative instability at the edge, which seems to be closely linked to the density limit in current-free devices, has not been observed. This is in line with the peculiarities of the cooling rate for Li atoms in the range of edge temperatures prevailing in the new scenario.

Clean plasmas are routinely obtained in TJ-II ECRH plasmas under low Z scenarios, largely due to the strong oxygen gettering effect of the B coatings and the use of graphite limiters [11]. Although the Li coatings were not aimed at improving this situation, a significant effect has been observed: the density-normalized signals from carbon emission, radiated power, neutral lithium and other impurity-related signals were seen to decrease during the operation day, accompanied by a concomitant evolution of particle recycling towards lower levels. A gradual improvement of the coating homogeneity by plasma erosion of the initial deposition spot may be responsible for the observed behaviour.

One of the main advantages of Li-coated walls, compared with former boronized walls, is the strong improvement of plasma density control by external puffing: the required puffing levels were significantly higher, by a factor of 2–3, for the same density; moreover, no sign of saturation was observed after a full day of ECRH operation. Particle balance yields a H retention under the Li coated walls a factor 4 higher than the B wall saturation limit. The dynamic behaviour of plasma particles during perturbative experiments shows that the effective fuelling is close to unity and the recycling coefficient $R < 0.20$. As a result, density control in NBI plasmas has been dramatically improved by the lithium coating. As an example, figure 1 shows the time evolution of some characteristic parameters for two representative examples of B and Li walls. In both cases ECH power is maintained along the full discharge even though the ECRH cut-off density is surpassed. As seen, an uncontrolled rise in electron density upon NBI takes place in the B case, leading to a rapid plasma collapse. For the Li example, however, a much better controlled density evolution can be achieved, with larger, stationary values of diamagnetic energy content, even when the high level of radiated power represents a larger sink of the available heating power in this case. The density control by external puffing in NBI plasmas is exemplified in figure 2, where the evolution of the plasma density during NBI heating for three consecutive discharges is displayed. Furthermore, no sign of collapse was seen up to central density values of 8×10^{19} m^{-3}, depending on the shape of the resulting plasma profile (see below). A key result is that particle fluxes to the wall during the NBI phase, as monitored by the Hα detectors located all over the machine, remain at the ECRH plasma level thus implying a strong enhancement (up to a factor of 4) of global particle confinement. This effect is also seen in the Li emission signal. The reference time for the density rise is the time when NBI is injected. This time is not unique, since it changes from one shot to another. For clarity, figure 2 now includes the NBI pulse and the puffing pulse. Although the initial rise is indeed higher just after the NBI launching, this is due to the overlapping with the gas pulse, which as seen in the figure, determines the final density value.

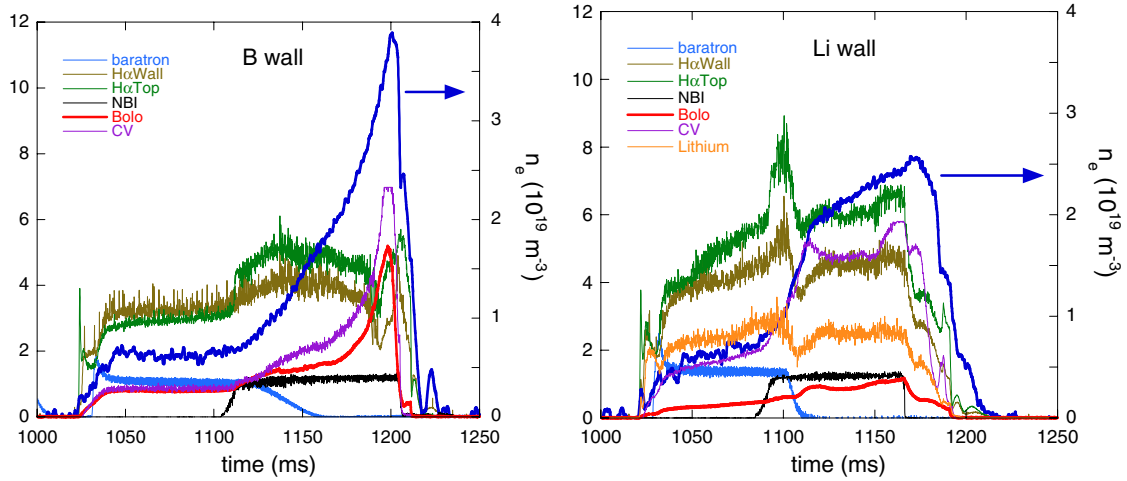

Figure 1. Time evolution of some characteristic parameters (line density, Hα emission from two monitors, CV emission, NBI signal, radiated power and baratron, i.e. puffed gas pressure) for two representative examples of B (left) and Li (right) walls.

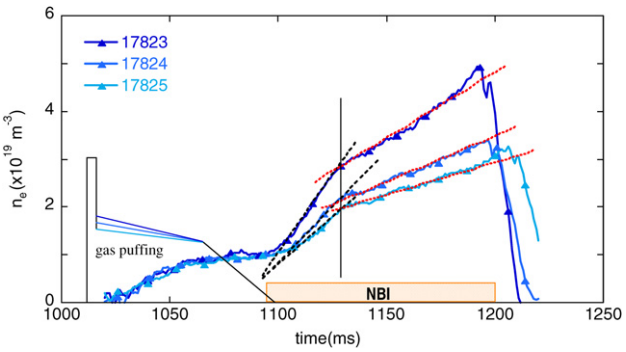

Figure 2. Evolution of the plasma line average density during NBI injection for three consecutive discharges, where the gas puffing has been varied. The NBI launching time window is also shown.

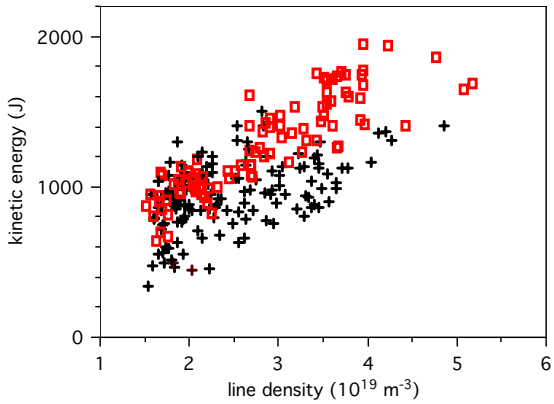

Figure 3. Plasma energy content versus line density for B (black pluses) and Li (red squares) coated-wall discharges in plasmas heated with only one NBI.

This feature was impossible in the B coated-wall scenario. Although not achieved in the series shown in figure 2, density (and $W_{\rm dia}$ and $P_{\rm rad}$) plateaus are produced in a routine way with Li walls. Hα and Li emission (when applicable) are shown in figure 1. As seen, after the transient rise upon heating beam injection, fluxes of Li and H decay to the previous ECRH level, even when the density is much higher.

As a consequence of the impurity composition and good particle confinement, total radiation levels are lower in the Li scenarios as compared with those obtained in boronized walls. Operation at the highest densities has been eased in the Li wall cases as compared with the B ones, which is a direct consequence of the lower threshold for plasma collapse existing in the latter case. Moreover, the development of plasma collapse follows a different pattern in both cases. Higher plasma energies at a given density were generally obtained under Li wall operation, as can be seen in figure 3, which shows the kinetic energy obtained from the plasma profiles for a selection of discharges heated with only one NBI in B and Li coated walls. Recently, operation with two NBIs (each supplying ~400 kW) has allowed an extension of the parameter range up to line densities above 6×10^{19} m^{-3} and kinetic energies of up to ~3 kJ, with the corresponding increment in the achieved plasma b. Operation with Li coating leads to two different radiation profiles (see figure 4) depending on fuelling strategy and local plasma parameters. The puffing strategy is chosen with a twofold purpose: to try to tailor the density profile in order to increase the NBI coupling and to control the density increase due to both puffing and NBI fuellings. In fact, it is seen in figure 2 that the time derivative of the line density is lower for lower puffing levels. It is not clear yet what are the recipes to get a bell or a dome shaped radiation profile. Nevertheless, it seems that the dome radiation profile is easier to obtain when NBI is launched on target plasmas with hollow density profile, and with low level of gas puffing.

For the broad, dome-type profile, central radiation levels are almost half of those observed in the peaked, bell-type counterpart. In spite of their lower total radiated power, development of the dome-type profile was systematically associated with a prompt plasma collapse. This fact can be found in the local power balance established at the plasma edge under central heating conditions. Indeed, the data shown in figure 4 indicate a significantly lower radiated power at the edge for the peaked, non-collapsing profiles. This balance has been called into play in defining the density limit in stellarators through the so-called 'low-radiative collapse' [12]. However, with the limited information presently available,

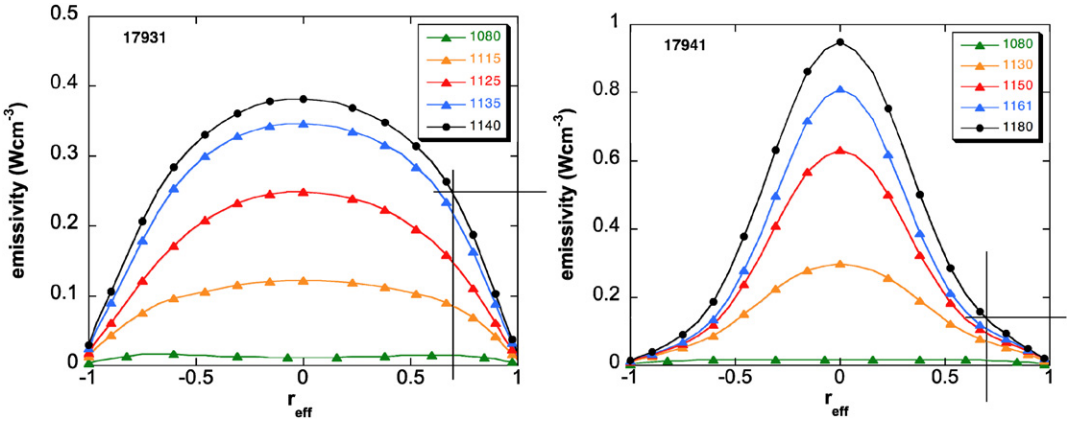

Figure 4. The two different radiation profiles, dome (left) and bell (right) type, found in NBI discharges depending on fuelling strategy and local plasma parameters.

another transport-based proposed mechanism for the density limit in stellarators cannot be ruled out.

The 3D structure of the ion collisional flux onto the vacuum chamber is obtained by means of the code ISDEP [13] showing that the groove is the preferred zone for the escaping particles to strike, in agreement with the experimental observations.

3. Confinement studies

3.1. Density and magnetic configuration scans

The effective electron thermal, χ_e, and particle, D, transport coefficient profiles have been studied through power and particle balance transport analysis. The energy confinement time τ_E increases linearly with density while the particle confinement time steps from low values $\tau_p \sim \tau_E$ to some four-fold values when crossing a density threshold ($\sim 0.6 \times 10^{19}$ m^{-3} in the standard magnetic configuration at ~400 kW ECRH power). This threshold is coincident with a change of sign in the radial electric field, from positive to negative, and is correlated with a qualitative change in ECRH-driven kinetic effects detectable in a clear drop in x-ray emissions above 20 keV at the threshold density [14]. The effective particle diffusivity decreases sharply at the threshold density in the outer half of the plasma—a more complete discussion on this density threshold will be given in the next paragraph. A proper interpretation of this phenomenon would require studying the change in collisional transport using self-consistent calculations of the radial electric field, including ECH driven kinetic effects. Even if the change in particle confinement time can be explained completely in terms of neoclassical transport, the experimental results show a clear change in the population of supra-thermal particles. Therefore, a complete account of the experimental results needs more than just the consideration of stable/unstable roots of the radial electric field, which makes the results different from the well-known electron/ion-root transitions.

The effective particle diffusivity decreases sharply at the threshold density in the outer half of the plasma—a more complete discussion on this density threshold will be given in the next paragraph. Within the same region, c_e decreases approximately in proportion to the line average density. Additionally, an interesting feature is that the lowest values for χ_e are found in regions in and around the location of lowest order magnetic resonances (see [15–17] for details). This is illustrated in figure 5, which consists of contour maps of χ_e profiles as the magnetic configuration changes either shot by shot or dynamically in a discharge with moderate (net currents up to ≈8 kA) ohmic induction. The radial location of magnetic resonances is indicated with lines. In figure 5 (left) the profiles correspond to a configuration scan [15] where the data were mostly taken from the Thomson scattering diagnostic. Each profile is the average of a few comparable discharges to line densities around 0.6×10^{19} m^{-3}. The positions of the two vacuum lowest order rational values of the rotational transform in this scan are drawn with lines (left: 8/5; right: 5/3). It is important to observe that, especially in a low magnetic shear machine like the TJ-II, a small alteration of the iota-profile can displace the location of these magnetic resonances in minor radius even if the net plasma current (bootstrap) in the static scan of figure 5 (left) is small, ~0.5 kA. To more deeply investigate this phenomenon, the same analysis was performed in dynamic experiments where a ramp in the ohmic transformer forces changes in the rotational transform profile, altering especially its shear [17]. In this case (see figure 5—right) the analysis was based on the time-resolved ECE diagnostic. The radial location of the main magnetic resonances is calculated using the measured net plasma current as boundary condition but considering only the ohmically induced currents. Again, the effect of a small—and evolving—bootstrap current could cause changes in the location of the resonances mostly in the inner half of the plasma and at the beginning of the discharges, when the magnetic shear is still small.

3.2. Confinement transitions in ECRH plasmas

In the previous section it was mentioned that, using the line density as a control parameter in ECRH plasmas, there is a substantial increment in particle confinement time accompanied by a change in the sign of the radial electric field. Therefore, this sign inversion can be associated with qualitative changes in confining properties and, possibly, turbulence. In fact, the inversion of the perpendicular rotation velocity of the turbulence from ion to electron diamagnetic direction [18] is directly connected to an inversion in the radial electric

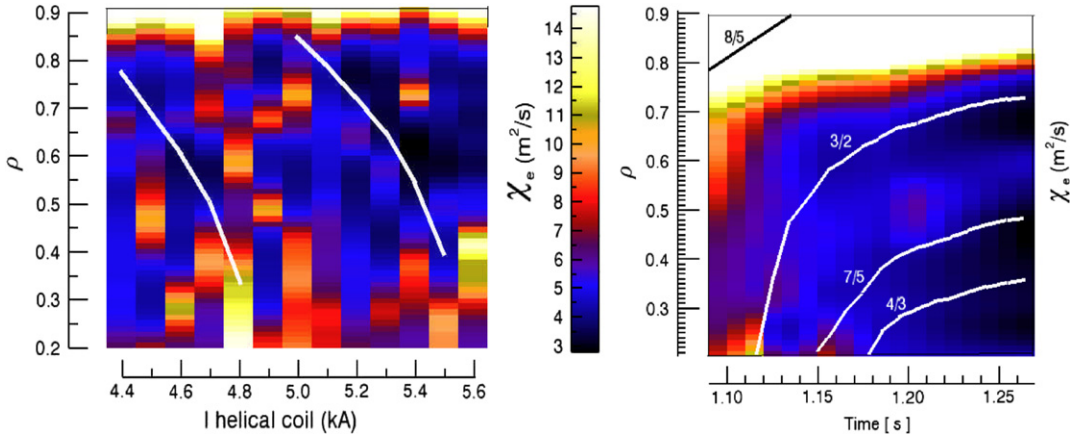

Figure 5. (Left) Profiles of the effective electron heat diffusivity χ_e for a configuration scan where the vacuum position (white lines) of the 8/5 (helical coil current range 4.4–4.8 kA) and the 5/3 (5.0–5.5 kA) magnetic resonances is varied in normalized minor radius ρ. (Right) Sequence in time of χ_e-profiles in a discharge with increasing negative ohmic plasma current, which causes several magnetic resonances to move through minor radius as shown with lines.

field and the development of the edge shear flows. It can be measured inside the plasma by reflectometry techniques [19] and CXRS [20] and by Langmuir probes in the plasma edge. It has been shown experimentally that the edge perpendicular plasma velocity of TJ-II reverses spontaneously when the line-averaged density reaches a certain threshold density in ECRH plasmas (see [21] and references therein) that depends on heating power and magnetic configuration. The analysis of direct measurements of electron density and temperature points to plasma collisionality as the magnitude that controls the inversion [22]. For constant temperature, there exists a density threshold to trigger such inversion. Above the threshold density, the turbulent structures (blobs) are stretched and ordered, the confinement improves and fluctuations and sheared flows are self-organized near marginal stability. TJ-II transitions have also been induced using an electrode that externally imposes a radial electric field at the plasma edge [23, 24].

In TJ-II, the steepest plasma gradients are located at the plasma radius $r \approx 0.7$ whereas the edge velocity shear layer is detected with probes located at $r \approx 0.9$. This decoupling between the locations of maximum gradient and edge sheared flows makes TJ-II a unique device to study the possible role of plasma gradients in the development of the universal edge sheared flows in fusion plasmas; measurements with a two-channel fast frequency hopping reflectometer have shown that the radial origin of the edge shear layer is the plasma region with maximum density gradient, expanding towards the edge until the edge shear flow is fully developed [25].

Different edge plasma parameters were simultaneously characterized in two different toroidal positions using two similar multi-Langmuir probes installed on fast reciprocating drives during spontaneous and biasing induced transitions to improved confinement regimes [26]. Edge sheared flows are developed at the same threshold density in the two different positions. Once sheared flows are developed fluctuation levels tend to decrease (figure 6). The long distance coupling between edge density and potential fluctuations has been investigated during transitions to improved confinement regimes in the TJ-II stellarator using the probes toroidally apart above mentioned.

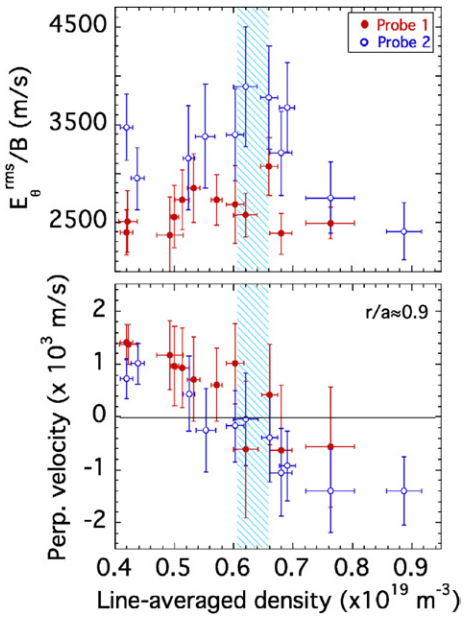

Figure 6. Averaged electric field fluctuations and perpendicular rotation velocity of the turbulence measured at two toroidal locations and at approximately the same radial position ($\rho \approx 0.9$) as a function of plasma density. The shaded areas in these two figures correspond to the critical density.

Results show a long distance correlation between floating potential signals that increases when probes are approximately at the same radial location, whereas there is no correlation between ion saturation current signals. Cross-correlation shows a maximum value when plasma density is close to the threshold for the development of spontaneous edge sheared flows $\approx 0.6 \times 10^{19}$ m^{-3} (figure 7). The increase in correlation with density results mainly from the rise in the correlation at low frequencies (below 20 kHz).

Edge sheared flows development has also been induced in TJ-II using an electrode that externally imposes a radial electric field at the plasma edge. Correlation between potential signals increases in plasma regimes with edge biasing induced enhanced confinement (figure 8). These findings show the

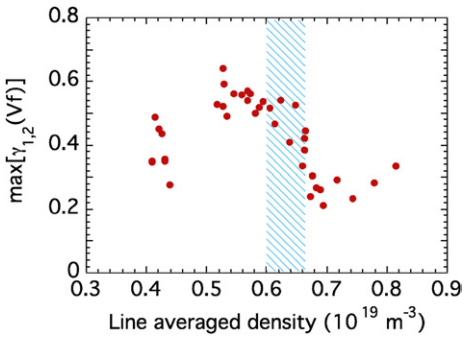

Figure 7. Maximum value of the cross-correlation between floating potential signals measured at approximately the same radial positions of both probes ($\rho \approx 0.9$) as a function of plasma density. As in figure 6, the shaded area corresponds to the critical density.

important role of long distance correlation as a first step in the transition to improved confinement regimes and the key role of electric fields to amplify them. Applying an external radial electric field was also seen to have a strong impact on the parallel Mach-number profile in the plasma edge [27]. Obtained results show the dual role of sheared $E \times B$ flows as a fluctuation stabilizing term as well as an agent affecting the parallel momentum balance via turbulence modification [28].

The behaviour of the bicoherence, computed for appropriate quantities such as the fluctuating poloidal electric field, shows an increase in non-linear coupling effects during biasing induced confinement transitions; however, this increase in the auto-bicoherence was significant only in a narrow radial range in contrast to the fluctuation levels which were affected over a very broad radial extension. A reduction in the Reynolds-stress component as a result of the lower turbulence level was observed. Nevertheless, the 'phase coherence' between the fluctuations was strongly enhanced inside the plasma.

Clarifying what mechanisms can provide such long-range correlations in plasma potential but not in density fluctuations remains an open question. Turbulence driven flows (zonal flows) are expected to show such correlations in the order parameter related to the shearing rate (i.e. electric fields through $E \times B$ flows) and so an amplification of such correlation via electric fields would also be expected. Actually, the experimental results can be theoretically understood by incorporating the dynamics of zonal flows into the second-order transition model for the emergence of the plasma edge sheared flow layer [29]. Ion orbit losses might also trigger localized perturbations in the plasma potential, whose parallel propagation could also trigger long-range correlations in potential fluctuations; however, in this case, it remains to be clarified why such particle orbit loss induced long-range correlations should be amplified by the electric fields. Comparative studies with other devices are crucial to assess the importance of multi-scale physics in the development of sheared flows and transport and the role of magnetic configuration (e.g. influence of safety factor).

3.3. Transitions in NBI plasmas

Operation under Li-coated wall conditions allows the plasma–wall interaction to decrease strongly with a subsequent reduction of CX, ionization and radiative losses at the edge [10]. Due to this new power balance and to the decrease in the neutral population, the experiments in NBI heated plasmas have shown evidence for additional transitions between the usual and improved confinement regimes, in which the plasma density and stored energy—measured, respectively, by interferometry and diamagnetic coils—increase spontaneously (see figure 9). The phenomenon shows typical features of the L–H confinement transitions observed in other devices: the confinement improvement is accompanied by a reduction in the Hα emission showing a decrease in the outward particle flux, together with the reduction in the level of broadband fluctuations, as measured by both reflectometry and Langmuir probes. Figure 10 shows the evolution of the electron density profile just before and after the transition, as measured by the Thomson scattering diagnostic for the four discharges shown in figure 9. A steeper density gradient is developed just at the transition. The electron temperature profile remains unchanged within the error bars, as does the ion temperature measured along a central plasma chord. It is worth mentioning that in TJ-II there is experimental evidence of the existence of a cold plasma edge region for all plasma conditions. As was shown in [30], more than 99% of the total plasma energy content is contained within $r \leqslant 0.9$ for many different magnetic configurations. This fact has been interpreted in terms of direct convective energy losses associated with ripple trapped heated particles [31] and explains the relatively internal position of the edge barrier in the present experiments.

The temporal evolution of the broadband fluctuations measured by reflectometry [19] is shown in figure 11 (bottom) together with the line density and the Hα signal (top). In this discharge, edge instabilities are developed about 10 ms after the L–H transition, as observed in Hα and reflectometry signals. These events propagate radially (inwards and outwards) with velocities in the range 1 km s^{-1}. H-mode transitions are realized at constant NBI heating power when the plasma density rises above a threshold level. They are observed at moderate input powers, with one and with two NBI injectors (about 400 kW port through, each); the threshold density being higher in the latter case. A similar threshold density was also found for the L–H transitions in the stellarator W7-AS [32]. So far, the H-mode has been obtained in a transient way: lasting several energy confinement times and ending with an increase in broadband fluctuations (figure 11) and a reduction in the stored energy (figure 9). The negative radial electric field (in the range 100 V cm^{-1}) developed during the low-density transition (described in section 3.2) becomes more negative after the L–H transition. The L–H transitions shown in figures 9–11 have been obtained in pure NBI heated plasmas with an input power of 400 kW; the absorbed power, estimated with the code FAFNER2 taking into account shine through, CX and ion losses, increases with plasma density and is about 50% of the input power at these densities ($\sim 2 \times 10^{19}$ m^{-3}). Although there exist uncertainties, it is worth noting that the absorbed power at the transition ($\sim$200 kW) is comparable to the power threshold calculated using the empirical scaling with plasma density ($n_e^{0.73}$), magnetic field ($B_t^{0.74}$) and plasma outer surface area ($S^{0.98}$) discussed in [33].

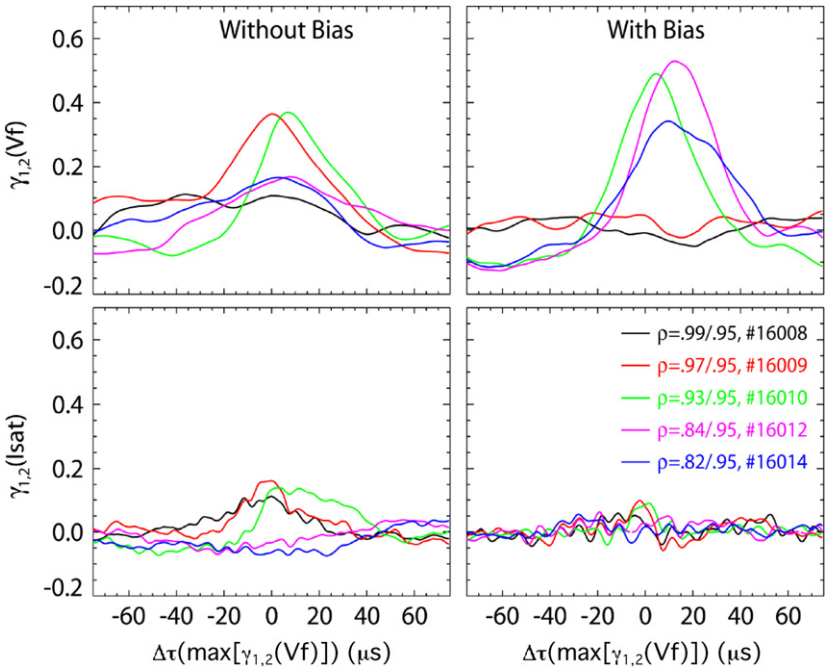

Figure 8. Cross-correlations of floating potential (top) and saturation current (bottom) without (left) and with (right) biasing for two probes located toroidally apart.

3.4. AE studies

NBI discharges present the appearance of AEs with frequencies of the order of hundreds of kilohertz, detected by Mirnov coils as well as by HIBP and reflectometry, thereby allowing the radial localization of the modes. Considering a typical density of $1.5 \times 10^{19}\,\mathrm{m}^{-3}$ and $B = 1\,\mathrm{T}$ being the magnetic field, the expected value of Alfvén velocity in a TJ-II hydrogen plasma is $v_\mathrm{A} \approx \left(B/\sqrt{\mu_0 n_\mathrm{i} m_\mathrm{i}}\right) = 6 \times 10^6\,\mathrm{m\,s}^{-1}$, where μ_0 is the vacuum magnetic permeability and n_i and m_i are the ion density and mass, respectively. TJ-II is equipped with a single array of 25 Mirnov coils located in a toroidal cross section measuring, roughly, the poloidal component of the magnetic field in the vicinity of the plasma column. This array provides information only on the 'm' poloidal number. The influence of AEs on fast ion confinement is studied using a fast ion luminiscent detector (FILD) that measures fast ion fluxes together with their pitch angle and energy [34]. Hα and FILD measurements show that AEs have an influence on fast ion confinement when they are located at outer radial positions $r > 0.6$. Low order rationals are found as key ingredients for AE destabilization and their influence on fast ion confinement [35]. As an example, figure 12 shows a Mirnov coil signal and its wavelet spectrogram together with the fast ions flux as measured by FILD in a pure NBI heated plasma for a magnetic configuration having a vacuum rotational transform equal to 1.65 at the plasma edge and 1.55 at the magnetic axis. A very short time window has been represented to highlight the intermittent character of the AEs and their correlation with fast ion flux. Two modes are destabilized simultaneously, both with $m = 5$ and with frequencies of 150 kHz and 200 kHz, respectively. The correlation between Mirnov coils and HIBP signals indicates that these modes are located at $r > 0.6$. These results indicate the existence of $n/5$ AEs in the plasma periphery which would be linked to the 8/5 rational surface present in the above mentioned vacuum rotational transform profile.

4. Summary

Considerable improvement of plasma particle control, in comparison with operation under boron coated walls, has been observed in the TJ-II stellarator after Li-coating. The beneficial Li properties for plasma–wall interaction have a strong effect on this device that has a helical limiter very close to the magnetic axis, which receives the strongest particle and heat fluxes. The outstanding results are density control in formerly collapsing NBI discharges and access to higher plasma pressures. The properties of Li as a plasma facing material in fusion devices are explored in these experiments, which are relevant for future fusion reactors, where Li could be used for liquid divertor or for coating some in-vessel components.

The technique used for lithiumnization is evaporation using ovens where the Li is homogenized about the vessel walls by the plasma itself. The wall properties after Li coating are strongly changed and, remarkably, they increase the H retention capability, thus improving the density control. Oxygen gettering is still maintained by the boron layer that is deposited under the Li one. A key ingredient for understanding the operational improvement is the change in profile radiation under Li coated wall. The edge radiation is observed to fall, which avoids the power imbalance that produces the low radiation collapse.

Confinement studies in ECH plasmas show that the lowest values for the effective electron heat diffusivity are found in regions where the lowest order magnetic resonances are located, while AEs destabilized in NBI plasmas, also related to low order resonances, can influence fast ion confinement.

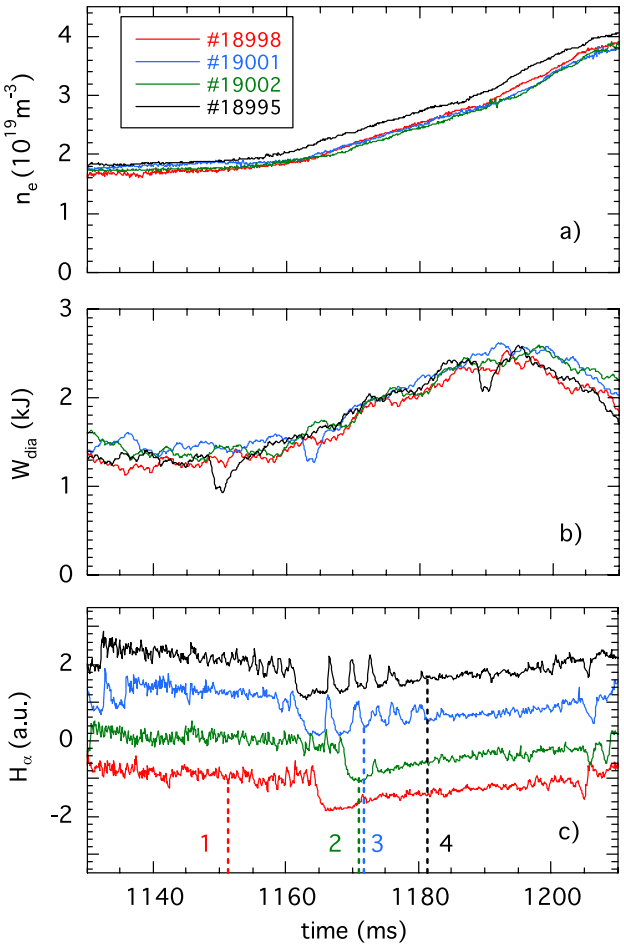

Figure 9. Time evolution of line density (*a*), diamagnetic energy (*b*) and Hα signal (*c*) in four similar discharges during the L–H transition. In (*c*), the vertical lines and the numbers, from 1 to 4, correspond to the time instants of the Thomson scattering diagnostic measurement in each discharge (the respective density profiles are shown in figure 10).

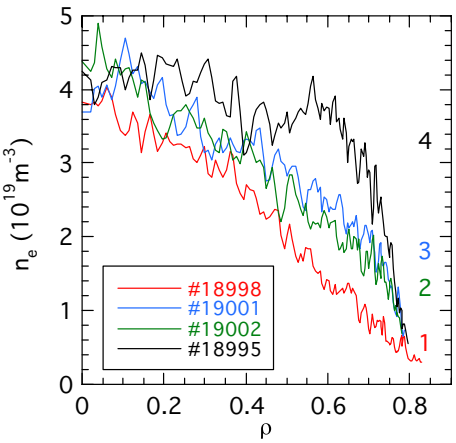

Figure 10. Evolution of the electron density profile during the L–H transition. The profiles are measured using the Thomson scattering diagnostic in the discharges and time instants shown in figure 9.

A transition from kinetic effect-dominated—with very low particle confinement times—to a more collisional regime is found in ECRH plasmas. The electric field, positive across the whole plasma in the low confinement regime, starts developing

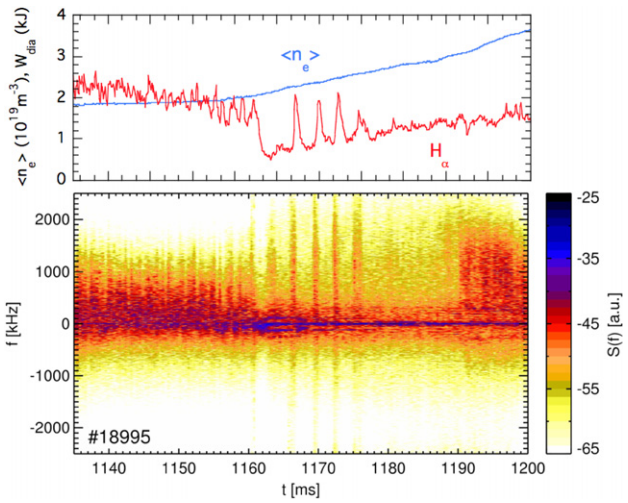

Figure 11. Time evolution of plasma density and Hα emission (top) and power spectra of broadband fluctuations measured by reflectometry (bottom) during the L–H transition.

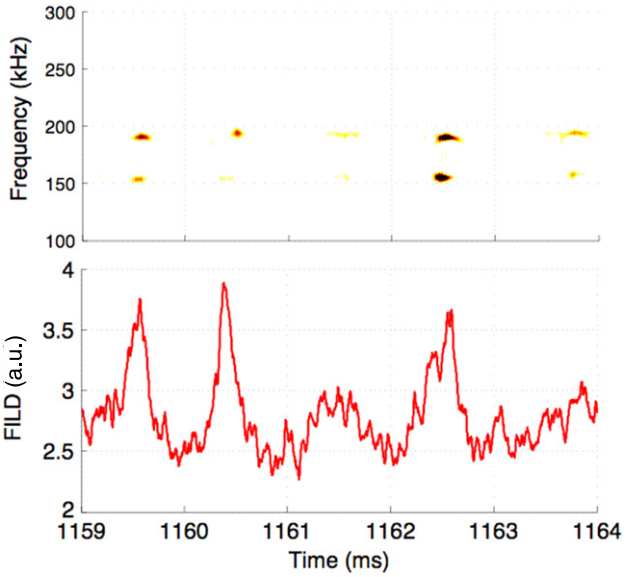

Figure 12. Wavelet spectrogram of a Mirnov coil signal (top) and flux of fast ions (bottom) in a pure NBI heated plasma in the standard configuration with vacuum rotational transform: 1.65 (edge)–1.55 (centre). The Alfven velocity in this discharge is around 6×10^6 m s^{-1} (see section 3.4)

negative values at the maximum density gradient region when the collisionality reaches a threshold value. For a given heating power and magnetic configuration, this translates into a line density threshold to improve particle confinement. Further increments in the density extend the region with negative electric fields towards the centre of the plasma.

During high density NBI operation, a transition to an improved confinement regime is observed, characterized by an increase in diamagnetic energy, a decrease in Hα emission, a drastic reduction in turbulence, and the development of steep density gradients. In some discharges, edge instabilities detected by Hα emission monitors, reflectometry and Langmuir probes, are triggered several milliseconds after the transition. So far, the H-mode has been obtained in a

transient way, and although it is subject to uncertainties, the estimated NBI absorbed power is comparable to the power threshold calculated using the empirical scaling obtained for tokamaks. This type of spontaneous transition adds to those that occur at lower densities, which correspond to the shear flow development and can also be provoked by biasing. During these lower density transitions, an increase in the cross-correlation in floating potential signals measured by probes located at distant toroidal positions is found. These results show that the increase in the degree of long-range correlation (for potential fluctuations) is strongly coupled to the presence of radial electric fields. The appearance of the L–H transition, at present under investigation, makes TJ-II a unique experiment to study the two-step process in the development of edge sheared flows in fusion plasmas, since both types of transitions are present in this device (see [36] and references therein).

References

[1] Sánchez J. *et al* 2007 *Nucl. Fusion* **47** S677–85
[2] Pericoli-Ridolfini V. *et al* 2005 *Plasmas Phys. Control. Fusion* **47** B258
[3] Kugel H.W. *et al* 2008 *Plasmas* **15** 056118
[4] Zakharov L.E. *et al* 2007 *J. Nucl. Mater.* **363–365** 453
[5] Wobig H. 2000 *Plasma Phys. Control. Fusion* **42** 931
[6] König R. *et al* 2004 *Fusion Sci. Technol.* **46** 152
[7] Maingi R. 2006 Magnetic field line tracing calculations for conceptual PFC design in NCSX *33rd EPS Conf. on Plasma Physics Controlled Fusion (Roma, Italy)*
[8] Castejón F., López-Fraguas A., Tarancón A. and Velasco J.L. 2008 *Plasma Fusion Res.* **3** S1009
[9] Tabarés F.L. *et al* 2007 Impact of lithium-coated walls on plasma performance in the TJ-II stellarator *Proc. 16th Int. Stellarator/Heliotron Workshop 2007 (Toki, Gifu, Japan, 15–19 October 2007)* I-20
[10] Tabarés F.L. *et al* 2008 *Plasma Phys. Control. Fusion* **50** 124051
[11] Tafalla D. and Tabarés F.L. 2002 *Vacuum* **67** 393
[12] Ochando M.A., Castejón F. and Navarro A.P. 1997 *Nucl. Fusion* **37** 225
[13] Castejón F. *et al* 2007 *Plasma Phys. Control. Fusion* **49** 753–76
[14] Vargas V.I. *et al* 2009 Density dependence of particle transport in ECH plasmas of the TJ-II stellarator *Ciemat Technical Report* 1162, February 2009 (https://www.etde.org/ and http://inisdb.iaea.org/inis/php/index.php)
[15] Vargas V.I. *et al* 2007 *Nucl. Fusion* **47** 1367–75
[16] Ascasíbar E. *et al* 2008 *Plasma Fusion Res.* **3** S1004
[17] López-Bruna D. *et al* 2008 *Europhys. Lett.* **82** 65002
[18] Hidalgo C., Pedrosa M.A., García L. and Ware A. 2004 *Phys. Rev.* E **70** 067402
[19] Estrada T., Blanco E., Cupido L., Manso M.E. and Sánchez J. 2006 *Nucl. Fusion* **46** S792
[20] Carmona J.M. *et al* 2008 *Plasma Fusion Res.* **3** S1044
[21] Pedrosa M.A. *et al* 2007 *Plasma Phys. Control. Fusion* **49** B303–11
[22] Guimarais L. *et al* 2008 *Plasma Fusion Res.* **3** S1057
[23] Pedrosa M.A. *et al* 2005 *Plasma Phys. Control. Fusion* **47** 777
[24] Hidalgo C. *et al* 2004 *Plasma Phys. Control. Fusion* **46** 287
[25] Happel T. Estrada T. and Hidalgo C. 2008 *Europhys. Lett.* **84** 65001
[26] Pedrosa M.A., Silva C., Hidalgo C., Carreras B.A., Orozco R.O., Carralero D. and TJ-II Team 2008 *Phys. Rev. Lett.* **100** 215003
[27] Alonso J.A. *et al* 2009 *Europhys. Lett.* **85** 25002
[28] Milligen Van B. *et al* 2008 *Nucl. Fusion* **48** 115003
[29] Carreras B., Garcia L., Pedrosa M.A. and Hidalgo C. 2006 *Phys. Plasmas* **13** 122509
[30] Ascasíbar E. *et al* 2005 *Nucl. Fusion* **45** 276
[31] Tabarés F.L. *et al* 2003 *J. Nucl. Matter.* **313–316** 839
[32] Wagner F. *et al* 2006 *Plasma Phys. Control. Fusion* **48** A217
[33] Ryter F. and the H-Mode Threshold Database Group 2002 *Plasma Phys. Control. Fusion* **44** A415
[34] Jiménez-Rey D. *et al* 2008 *Rev. Sci. Instrum.* **79** 093511
[35] Jiménez-Gómez R. *et al* 2009 Alfvén eigenmodes measured in the TJ-II stellarator *Nucl. Fusion* submitted
[36] Terry P. 2000 *Revi. Mod. Phys.* **72** 109